Modeling of Oxygen Mass Transfer in a Gas–Liquid Airlift Reactor

Samuel Talvy, Arnaud Cockx, and Alain Liné
Laboratoire d'Ingénierie des Systèmes Biologiques et des Procédés (LISBP) UMR INSA-CNRS 5504, UMR INSA-INRA 792, 31077 Toulouse cedex, France

DOI 10.1002/aic.11075
Published online January 3, 2007 in Wiley InterScience (www.interscience.wiley.com).

This article focuses on the physical modeling and numerical simulation of mass transfer in two-phase bubbly flow in an airlift internal loop reactor. The objective of this article is to show the ability of computational fluid dynamics (CFD) to correctly simulate mass transfer in such a bubbly reactor. The modeling of two-phase bubbly flow is based on the so-called two-fluid model derived from Reynolds-averaged Navier–Stokes equations in two-phase flow. From the hydrodynamic perspective, the flow is steady state. Given the steady-state distributions of phases, interfacial area, and velocity field in the whole volume of the airlift, mass transfer is computed and the evolution of oxygen concentration in the two phases is predicted. Numerical simulations are discussed after comparison to experimental data. The simulations are validated in terms of oxygen concentration in the liquid vs. time. Then, different points are discussed, in particular, the perfectly mixed reactor assumption in the liquid phase and the spatial and temporal heterogeneity of oxygen concentration in the gas arising from oxygen impoverishment in bubbles in the downcomer. This leads to heterogeneity of the transfer driving force between the gas and the liquid. Bubble age or residence time in the airlift loop reactor has been calculated to show the weak renewal of oxygen in bubbles in the downcomer. This discussion generates questions on the estimation of a global mass transfer coefficient from experiments in such a heterogeneous airlift reactor. *AIChE J,* 53: 316–326, 2007
Keywords: airlift, hydrodynamics, mass transfer, two-phase flow, computational fluid dynamics (CFD)

Introduction

The scope of the present study is related to water and wastewater treatment. Gas–liquid reactors are mainly used to achieve mass transfer. In particular, bubbly flows are frequently chosen because of their high interfacial area. Examples of application to water and wastewater treatment are ozonation[1–3] and bioreactors.[4,5] In these processes, mass is transferred from a dispersed gas phase (air bubble) to a continuous liquid phase (water).

In chemical engineering, the global mass transfer efficiency of an airlift reactor is usually expressed by a global mass transfer coefficient k_La_L. To better understand the meaning of mass transfer coefficient, and then to improve its determination, the use of computational fluid dynamics (CFD) is actually helpful.

To evaluate k_La_L by experiment or by simulation, oxygen is removed from the liquid by adding sodium sulfite. As soon as all the sodium sulfite is consumed, the oxygen recovery in the liquid is measured and is directly related to the mass transfer coefficient k_La_L. Because the airlift is assumed to be a perfectly mixed reactor as a bubble column,[6] the global equation of concentration evolution is given by

$$\frac{dC_L}{dt} = k_La_L(C_L^* - C_L) \quad (1)$$

Correspondence concerning this article should be addressed to A. Liné at alain.line@insa-toulouse.fr.

The mathematical solution is

$$C_L = C_L^*(1 - \exp^{-k_L a_L t}) \tag{2}$$

Thus, it is usual to determine the global mass transfer coefficient $k_L a_L$ by fitting the plot of oxygen concentration in the liquid vs. time. Previous studies addressing this issue[7–9] proposed a model that assumes (1) plug flow in the riser and in the downcomer and (2) that oxygen concentration is constant in the gas. Airlift reactors have been proven to perform efficient mass transfer.[3,10]

The objective is to simulate mass transfer in this airlift loop reactor. The numerical results are compared to experiments acquired from laboratory pilot-scale studies.[11] In a second part, model equations and closure relations are presented. Next, the Experimental section deals with oxygen concentration measurements in the liquid phase. The simulations are validated against experimental data in a later section. Closure modeling on interfacial area and mass transfer coefficient are discussed. The final section treats the heterogeneity of mass transfer, gas oxygen concentration, and bubble age in the airlift reactor.

Mathematical Modeling

In this study, the two-fluid model has been validated in the airlift reactor.[12] The steady-state hydrodynamic solution of the air–water flow in the airlift is considered as input data for the present article. Consequently, only the transport equations of concentration in two-phase flow will be briefly reviewed.

To perform the mass transfer experiment from a numerical perspective, it is first necessary to recall the equation governing the concentration transport phenomena. As the result of turbulence, local instantaneous concentration and velocity are decomposed as

$$c_k = \overline{C_k} + c_k' \qquad \text{and} \qquad u_k = \overline{U_k} + u_k' \tag{3}$$

where the overbar denotes Reynolds average and the prime denotes turbulent fluctuations. Thus, the general transport equation of the concentration in two-phase flow is given by

$$\frac{\partial \alpha_k \overline{C_k}}{\partial t} + \nabla \cdot \alpha_k \overline{C_k U_k} = \alpha_k S_k - \nabla \cdot \alpha_k (\overline{J_k} + \overline{c_k' u_k'}) + \overline{c_k m_k} + \overline{L_k} \tag{4}$$

where $\alpha_k S_k$ represents a source term linked to the consumption or production of the concentration c_k. $\overline{L_k}$ represents the interfacial transfer of concentration between the two phases:

$$\overline{L_k} = -\overline{J_k n_{ik} \delta_i} \tag{5}$$

and $\overline{L_k}$ represents the molecular diffusion modeled by Fick's law:

$$\overline{J_K} = -D_k \nabla \cdot C_k \tag{6}$$

Finally, $\overline{c_k m_k}$ represents the transport of concentration c_k by mass transfer.

Closure of turbulence

The turbulent diffusion of the concentration in the liquid is expressed in terms of turbulent diffusivity D_{tL}:

$$-\overline{c_L' u_L'} = D_{tL} \nabla \overline{C_L} \tag{7}$$

where the turbulent diffusivity D_{tL} is proportional to the turbulent viscosity and has the same order of magnitude:

$$D_{tL} = \frac{\nu_{tL}}{\mathrm{Sc}_t} \tag{8}$$

with a turbulent Schmidt number $\mathrm{Sc}_t \approx 1$. It expresses that the same turbulent structures diffuse both the momentum and the concentration attached to fluid particles.

Closure of interfacial mass transfer

The interfacial mass transfer between the gas bubbles and the liquid is expressed in terms of interfacial area a and transfer velocity k_L, usually called transfer coefficient.

$$\overline{L_L} = k_L a \left(C_L^* - \overline{C_L}\right) \tag{9}$$

In Eq. 9, a is the interfacial area, which can be written as

$$a = \alpha_G \frac{S_b}{V_b} \tag{10}$$

where S_b is the surface of the bubbles and V_b represents their volume. In the case of a sphere, the ratio $S_b/V_b = 3/r_b$. Thus, in the case of spherical bubbles, the interfacial area is expressed as

$$a = \frac{3\alpha_G}{r_b} \tag{11}$$

In an airlift reactor, the characteristic scale controlling the mass transfer is probably related to the bubbles. The timescale is thus the ratio of the bubble diameter d_b over the relative velocity $\overline{U_r}$:

$$t_b = \frac{d_b}{\overline{U_r}} \tag{12}$$

The transfer coefficient k_L can thus be estimated by the classical (1935) penetration theory of Higbie.[13] Thus a local term for the transfer is introduced:

$$k_L = \frac{2}{\sqrt{\pi}} \sqrt{\frac{D_L U_r}{d_b}} \tag{13}$$

where D_L is the molecular diffusion of oxygen in water.

In Eq. 9, C_L^* is the saturation concentration in water and is generally given by Henry's law:

$$C_L^* = \mathrm{He} P_{\mathrm{O}_2} \tag{14a}$$

where He is the Henry constant representing oxygen solubility in water (1.05×10^{-5} mol m^{-3} Pa^{-1} at 25°C). For a pressure in the gas of 1 atm, $C_L^* = 8$ mg/L.

$$P_{O_2} = 0.21 P_g \tag{14b}$$

Table 1. Experimental Data after Couvert (2000)

Gas flow rate (L/s)	0.62	2.12	5.62
Superficial gas velocity (cm/s)	0.5	1.7	4.5
Mean gas fraction	0.8	2.6	7.0
Mean gas fraction in the riser	1.1	3.7	7.8
Mean gas fraction in the downcomer	0.6	1.8	6.5
Bubble Sauter diameter (mm)	2.7	3.4	4.3

In the present case, the local saturation concentration C_L^* can be estimated from Henry's Law and the local concentration of oxygen in the gas $\overline{C_G}$.

$$C_L^* = m\overline{C_G} \tag{15}$$

with m defined as follows:

$$m = \mathrm{He}RT \tag{16}$$

where R is the ideal gas constant and T is the temperature.

Oxygen transfer model equation in bubbly flow

In the simulation, the initial condition corresponds to the complete consumption of sulfite in the airlift and thus the initial simulated concentration of oxygen in the liquid is null. The oxygen is transferred from the air bubble to the water:

- Transport equation of oxygen in the gas

$$\frac{\partial \alpha_G \overline{C_G}}{\partial t} + \nabla \cdot \alpha_G \overline{C_G}\,\overline{U_G} = -k_L a(m\overline{C_G} - \overline{C_L}) \tag{17}$$

- Transport equation of oxygen in the liquid

$$\frac{\partial \alpha_L \overline{C_L}}{\partial t} + \nabla \cdot \alpha_L \overline{C_L}\,\overline{U_L} = \nabla \cdot \alpha_L[(D_L + D_{tL})\nabla \overline{C_L}] + k_L a(m\overline{C_G} - \overline{C_L}) \tag{18}$$

These two equations are closely coupled because the transfer depends on $(C_L^* - \overline{C_L}) = (m\overline{C_G} - \overline{C_L})$ and $C_L^* = m\overline{C_G}$ is a linear function of the concentration of oxygen in the gas.

Experimental

The experimental pilot and Fluent® code (Fluent Inc., Lebanon, NH) were presented in a previous article.[12] The reactor, a parallelepiped vessel (3 m high and 0.5 m wide and deep), is equipped with a baffle in its middle. The baffle position is fixed. The reactor was initially filled with tap water up to 2.6 m high. The pilot is divided into four sections: an upward flow-aerated section, the free surface flow above the internal wall, a downward flow less aerated section usually called downcomer, and the flow below the internal wall including the gas injector usually called sparger. The liquid height below the internal wall is 150 mm. The experimental results of mass transfer referred to in this article were obtained by Couvert.[11] To evaluate mass transfer by experiments, oxygen is removed from the liquid by addition of sodium sulfite. As soon as all the sodium sulfite is consumed, the oxygen recovery in the liquid is measured and is directly related to the mass transfer. Two superficial gas velocities will be simulated (1.7 and 4.5 cm/s; Table 1) and are compared to experimental results plotted in Figures 1a and 1b.

A typical analysis of the plot of concentration vs. time (Figure 1) consists in fitting the curve with an exponential function, because of the perfectly mixed behavior (Eq. 2):

$$\overline{C_L}(t) = \overline{C_L}(t_\infty)\left(1 - e^{-t/\tau}\right) \tag{19}$$

Considering the previous expression, the timescale τ correspond to a relaxation time of mass transfer, given that when $t = \tau$, the concentration of oxygen in the liquid is equal to 63% of its maximum value $\overline{C_L}(t_\infty)$:

$$\frac{\overline{C_L}(\tau)}{\overline{C_L}(t_\infty)} = 1 - \frac{1}{e} = 0.63 \tag{20}$$

From Figure 1, one notices that different values of the relaxation time have been imposed. For the superficial gas velocity 1.7 cm/s, the three curves correspond to Eq. 19, with τ^{-1} values of 0.015, 0.017, and 0.02 s^{-1}. For the superficial gas velocity 4.5 cm/s, the three curves correspond to τ^{-1} values of 0.03, 0.035, and 0.04 s^{-1}. In all cases, $\overline{C_L}$ (t_∞) is fixed to 8 mg/L.

From Figure 1a, one can see that during the first 70 s, the experimental data follow a τ^{-1} value of 0.017, whereas after 70 s, it

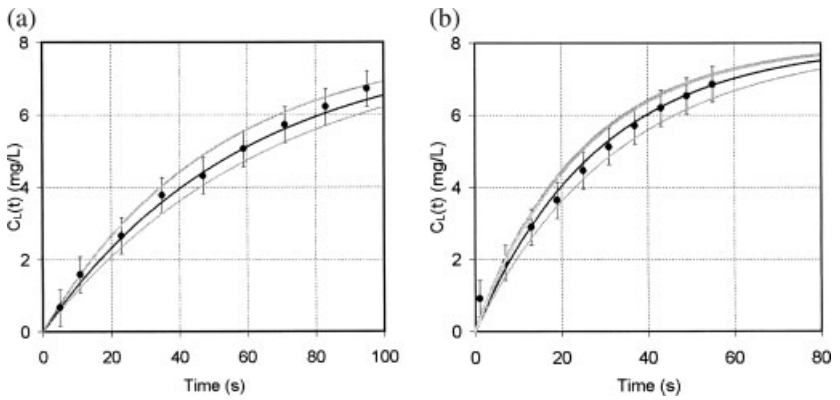

Figure 1. Global concentration of dissolved oxygen with different values of τ^{-1}.

(a) For j_G = 1.7 cm/s: ● Experiment; ▬ 0.02 s^{-1}; — 0.017 s^{-1}; ▬ 0.015 s^{-1}. (b) For j_G = 4.5 cm/s: ● Experiment; ▬ 0.04 s^{-1}; — 0.035 s^{-1}; ▬ 0.03 s^{-1}.

follows a τ^{-1} value of 0.020. The difference is not too large, although the τ^{-1} value does not seem to be constant. In Figure 1b, the experimental data follow the previous behavior, with a constant τ^{-1} value of 0.035.

In the present case, for a superficial velocity of 1.7 cm/s, the relaxation time ranges from 60 to 65 s; at this time, the concentration in the liquid is 5 mg/L, which is almost 63% of the saturation concentration (8 mg/L). Comparing this transfer timescale (60 s) to the macromixing timescale (100 s), mixing may interact with mass transfer. Thus, the assumption of a completely mixed reactor seems questionable. Similarly, for a superficial velocity of 4.5 cm/s, the relaxation time of mass transfer is 30 s. In this case, the macromixing timescale is 75 s. Thus, mixing may again interact with mass transfer.[12] Usually, the inverse timescale τ^{-1} is interpreted in terms of global mass transfer coefficient k_La value. This will be discussed below.

Validation of Numerical Simulation of Mass Transfer

In this paragraph, different closure relations are discussed. First, interfacial area (a) depends on bubble shape. In our experiments, bubbles are not spherical, but ellipsoidal; thus interfacial area should be affected by bubble distortion. Second, mass transfer coefficient (k_L) is discussed and its order of magnitude is quantified.

Discussion on closure strategy

Interfacial Area. The interfacial area given by Eq. 10 can be reconsidered in the case of ellipsoidal bubbles. In a previous article[12] on hydrodynamics in the airlift, the ellipsoidal shape of the bubbles was shown to be significant in estimation of the drag coefficient. The purpose here is to estimate whether the ellipsoidal shape of the bubbles is also important in terms of mass transfer interfacial area. Assuming an ellipsoidal shape for the bubble with a circular horizontal projected area (diameter b) and a vertical smaller axis c, noting $E = c/b$, the interfacial area is

$$a = \frac{3\alpha_G}{r_{beq}} f(E)$$

- Volume of the ellipsoid

$$V_b = \frac{4}{3}\pi b^2 c = \frac{4}{3}\pi \frac{c^3}{E^2} = \frac{4}{3}\pi r_{beq}^3 \tag{21}$$

- Surface of the ellipsoid

$$S_b = \tau\, r_{beq}^2 E^{4/3}\left[\frac{2}{E^2} + \frac{1}{\sqrt{1-E^2}}\ln\left(\frac{1+\sqrt{1-E^2}}{1-\sqrt{1-E^2}}\right)\right] \tag{22}$$

Thus, the interfacial area is given by Eq. 23, where the corrective factor f is given by

$$f(E) = \frac{E^{4/3}}{4}\left[\frac{2}{E^2} + \frac{1}{\sqrt{1-E^2}}\ln\left(\frac{1+\sqrt{1-E^2}}{1-\sqrt{1-E^2}}\right)\right] \tag{23}$$

For superficial velocities of 0.5, 1.7, and 4.5 cm/s, diameters of the bubbles[12] are 2.7, 3.4, and 4.3 mm and, following Clift et al.,[14] the eccentricities are, respectively, 0.43, 0.36, and 0.28, leading to corrective factors of 1.15, 1.20, and 1.35. Thus, the difference of ratio S_b/V_b between a sphere and an ellipsoid (between 15 and 30%) remains small compared to the difference of apparent drag coefficient (up to 200%), but may be nonnegligible.

Neglecting the corrective factor, the interfacial area can be estimated for each superficial velocity. In the riser, for superficial velocities of 0.5, 1.7, and 4.5 cm/s, the gas fraction is of the order of 1, 4, and 8%; thus the interfacial areas are, respectively, 22, 70, and 111 m^2/m^3. Accounting for the corrective factor, the interfacial area becomes 25, 84, and 150 m^2/m^3. Similarly, in the downcomer, for gas superficial velocities of 0.5, 1.7, and 4.5 m/s, the gas fraction in the aerated region is of the order of 0, 6, and 10%[12]; thus, neglecting the corrective factor, the interfacial areas are, respectively, 0, 105, and 140 m^2/m^3 in aerated regions (representing 0, 40, and 60% of the downcomer). Accounting for the corrective factor, the interfacial area in the aerated region of the downcomer becomes respectively 0, 126, and 189 m^2/m^3. The sensitivity of simulated oxygen concentration in the liquid to the corrective factor needs to be discussed.

Mass Transfer Coefficient. The mass transfer coefficient k_L is estimated by the classical penetration theory of Higbie,[13] given by Eq. 13. For the three bubble diameters (2.7, 3.4, and 4.3 mm) having a similar relative velocity close to 0.25 m/s, the transfer coefficient k_L values are, respectively, 4.6, 4.1, and 3.6×10^{-4} m/s.

In airlift, the flow of liquid being turbulent, the turbulence in the liquid can increase the mass transfer. The question is how it may be affected. To assess the mass transfer value, one can calculate the mass transfer in the case of turbulent flow, using the expression proposed by Lamont and Scott[14]:

$$k_L = 0.4\ \mathrm{Sc}^{-1/2}(\nu_L\varepsilon_L)^{1/4} \tag{24}$$

where

$$\mathrm{Sc} = \frac{D_L}{\nu_L}$$

The dissipation rate of turbulent kinetic energy can here be estimated from gas flow:

$$\varepsilon_L = j_G g \tag{25}$$

where j_G is the superficial velocity of gas.

For the three superficial gas velocities (0.5, 1.7, and 4.5 m/s) having a similar molecular Schmidt number of 500, the transfer coefficient k_L values are, respectively, 2.7, 3.6, and 4.6×10^{-4} m/s. Surprisingly, the same order of magnitude is obtained from Eqs. 24 and 13. Thus, using the correlation proposed by Higbie[13] will ensure a correct order of magnitude of the mass transfer coefficient k_L, even if the role of turbulence on mass transfer of gas between bubbles and liquid is not accounted for.

In the literature, another expression of mass transfer coefficient derived from Bird et al.[16] is used.[17] This expression is given in terms of Sherwood number (Sh), as

$$\mathrm{Sh} = \frac{k_L d_b}{D_L} = 2 + 0.6415(\mathrm{Re}\ \mathrm{Sc})^{1/2} \tag{26}$$

Thus, it can be written in terms of mass transfer coefficient as

$$k_L = \sqrt{\frac{4}{3\pi}}\ \sqrt{\frac{D_L U_r}{d_b}} \tag{27}$$

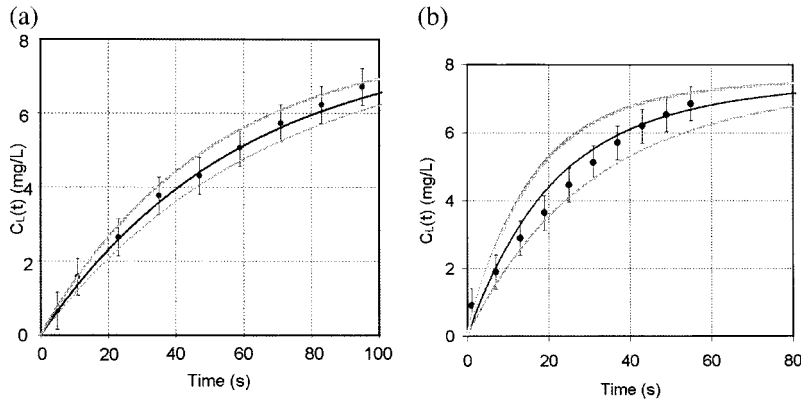

Figure 2. (a) Concentration of dissolved oxygen according to interfacial area calculation (j_G = 1.7 cm/s); (b) concentration of dissolved oxygen according to interfacial area calculation (j_G = 4.5 cm/s).

● Experiment, — eccentricity correction, without eccentricity correction, with eccentricity correction + wake effect.

This expression, derived by Bird et al.[16] for mass transfer of creeping flow around a gas bubble, concerns values of mass transfer coefficient half the value at relatively high Reynolds number given above and close to 4×10^{-4} m/s. Consequently, the relation proposed by Higbie[13] will be used in the present work.

Validation of prediction of mass transfer from gas bubble to liquid

The initial conditions correspond to the instant when all the sodium sulfite has been consumed. The initial concentration of oxygen in water is thus 0 mg/L. The inlet concentration of oxygen in the gas at the injector is fixed at 310 mg/L. The initial concentration of oxygen in the gas bubble is more difficult to estimate; it has been assumed to be the same as the concentration at the injector, that is, 310 mg/L.

In the CFD approach, because the hydrodynamics is in a steady state, only two transport equations of concentration, Eqs. 17 and 18, are solved, to predict mass transfer in the airlift reactor. One equation concerns the oxygen concentration in bubbles; the other equation corresponds to the oxygen concentration in water.

Numerical probes are placed in the riser and in the downcomer, to measure oxygen concentrations with time, for both liquid and gas phases, and to compare simulation to experimental data. Transient evolutions of the spatial averages of both oxygen concentrations in the gas and in the liquid are also recorded.

Two superficial gas velocities are simulated (1.7 and 4.5 cm/s).

Spatial Average of Oxygen Concentration in the Liquid vs. Time. Because the airlift reactor is assumed to be perfectly mixed, the spatial average of oxygen concentration in the liquid is first addressed. The increase of spatial average oxygen concentration in the liquid is plotted vs. time (Figures 2a and 2b) for each superficial gas velocity (1.7 and 4.5 cm/s). The spatial average oxygen concentration in the liquid is compared to experiments.

In both cases (1.7 and 4.5 cm/s), simulations are in good agreement with experiments. The black lines correspond to an interfacial area without corrective factor. It means that the interfacial area is equal to the interfacial surface of a sphere whose volume is equal to the volume of the ellipsoidal bubble. Because of the distortion of the bubble, this estimation may be inaccurate. A sensitivity analysis is presented in terms of interfacial area. The thick gray curves correspond to interfacial area including the corrective factor (1.2 and 1.35, respectively). In these cases, mass transfer is increased because the interfacial area of an ellipsoid is geometrically increased. In fact, this may be true in creeping flow conditions, but at larger Reynolds number; because of the wake, the geometrical interfacial surface probably overestimates

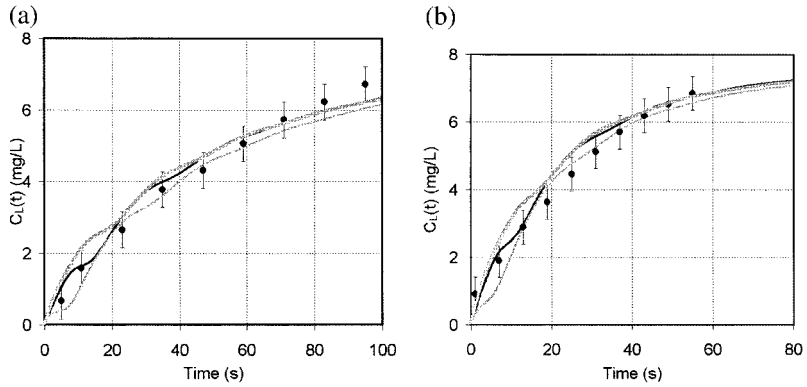

Figure 3. (a) Local concentration of dissolved oxygen (j_G = 1.7 cm/s); (b) local concentration of dissolved oxygen (j_G = 4.5 cm/s).

● Experiment, — 2 m in downcomer, 2 m in riser, 0.5 m in riser.

Table 2. k_La_L and τ^{-1} Values in Riser and Downcomer

			Riser			Downcomer			Mean			
j_G (cm/s)	d_b (mm)	k_L (m/s)	α_G (%)	a (m^2/m^3)	k_La_L (s^{-1})	α_G (%)	a (m^2/m^3)	k_La_L (s^{-1})	α_G (%)	a (m^2/m^3)	k_La_L (s^{-1})	Experimental τ^{-1} (s^{-1})
1.7	3.4	4.1×10^{-4}	3.7	65	0.028	2.5	44	0.018	3.1	55	0.023	0.017
4.5	4.3	3.6×10^{-4}	7.8	109	0.042	6.5	91	0.033	7.15	99	0.038	0.035

the effective interfacial area of mass transfer.[18] Blanco and Magnaudet[18] showed by direct numerical simulation around an ellipsoidal bubble that the separation angle varies between 130 and 170° for bubble Reynolds number between 200 and 1000. The thin gray curves correspond to interfacial area including wake effect, with corrective factor arbitrarily fixed to 0.8 and 0.65.

The truth is probably located between the gray curves. Our purpose is not to close the problem of mass transfer interfacial area modeling, but to highlight that the relative agreement between simulated black curves and experiments probably results from a balance between increase of geometrical interfacial area of the ellipsoid and decrease of the effective mass transfer area arising from wake.

Local Oxygen Concentration in the Liquid vs. Time. In the Experimental section, the assumption of perfectly mixed reactor was questioned. To clarify this point, oxygen concentrations measured in the liquid, predicted in different locations, are plotted in Figures 3a and 3b, for each superficial gas velocity (1.7 and 4.5 cm/s). The different numerical probes show a similar trend, indicating that the reactor globally behaves as a mixed reactor.

A more detailed analysis shows that low frequency is superimposed onto the global trend. The period of modulation is close to the circulation time ($\approx$25 s). These modulations do not appear in the experiments because the frequency of acquisition is too low and filters these fluctuations.

Conclusion. The two-phase flow hydrodynamics having been validated in a previous article,[12] the present results validate the modeling of the interfacial transfer, related to the mass transfer coefficient k_L, the simplified interfacial area a, and the saturation concentration C_L^*. It also validates the simulations in two dimensions.

However, the numerical data can be helpful to better understand the mass transfer phenomena in the airlift.

Because the inverse relaxation timescale τ^{-1} is usually interpreted in terms of the global mass transfer coefficient k_La_L value, it is interesting to compare the experimental and simulated τ^{-1} values to the modeling of k_La_L. The mass transfer coefficient can be estimated from interfacial area and gas fraction in the airlift, in the riser, and in the downcomer. Recall that the estimation of modeled local mass transfer is

$$k_La_L = \frac{6\,\alpha_G}{\alpha_L\, r_b}\sqrt{\frac{D_L U_r}{\pi\, d_b}} \tag{28}$$

Given the gas fraction in the riser and in the aerated part of the downcomer (from the CFD), it is thus possible to estimate the local modeled mass transfer.

From Table 2, the first important result is that the experimental values of mass transfer coefficient (right column) are 0.017 and 0.035 s^{-1} (see Experimental section) and do not correspond to the mean value of the modeled mass transfer coefficients, respectively 0.023 and 0.038 s^{-1}. This discrepancy will be explained by the heterogeneity of mass transfer in the airlift.

The second result is that the values of modeled mass transfer coefficients in the riser and in the downcomer are very different. For a superficial gas velocity of 1.7 cm/s, the mass transfer coefficient is 0.028 s^{-1} in the riser and 0.018 s^{-1} in the downcomer. For a superficial gas velocity of 4.5 cm/s, the mass transfer coefficient is 0.042 s^{-1} in the riser and 0.033 s^{-1} in the downcomer. All these differences indicate that mass transfer is not uniform throughout the whole volume of the airlift.

A second element related to the nonuniformity of the mass transfer is shown in Figure 4a, where the spatial average of oxygen concentration in the gas is plotted vs. time and in Figure 4b, where the volume average transfer driving force is plotted vs. time.

Figure 4a shows that the spatial average of oxygen concentration in the gas (initially 310 mg/L) is not constant with time, but decreases to 285 mg/L at the superficial gas velocity of 4.5 cm/s and to <270 mg/L at the superficial gas velocity of 1.7 cm/s.

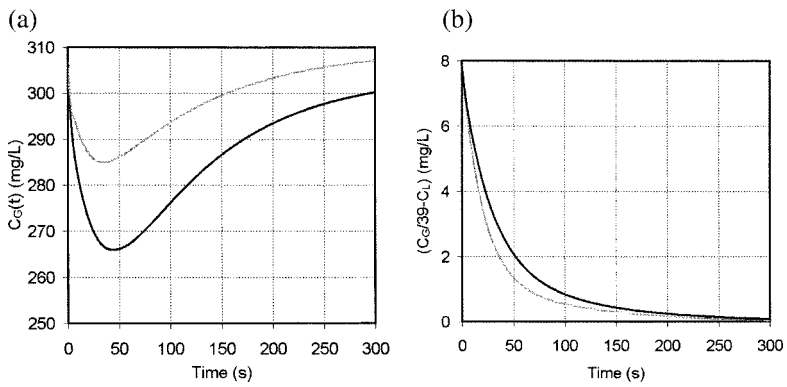

Figure 4. (a) Global oxygen concentration (C_G) evolution; (b) global transfer driving force evolution.

— j_G = 1.7 cm/s, ····· j_G = 4.5 cm/s.

This result seems surprising and will be explained in the next paragraph. The main consequence is that the saturation concentration C_L^* is not constant either.

If the saturation concentration was constant, the transfer driving force should be expressed as

$$C_L^* - \overline{C_L} = C_L^* e^{-(t/\tau)} \tag{29}$$

When t equals the relaxation time τ, the transfer driving force, given by the previous relation,[33] would equal 36% of C_L^*. If the saturation concentration C_L^* is constant and equal to 8 mg/L, then 36% $C_L^* = 2.9$ mg/L. For a superficial velocity of 1.7 cm/s, the relaxation time is 60 s and the transfer driving force given by the simulation (Figure 4b) at this time is 1.7 mg/L, thus smaller than 2.9 mg/L. For a superficial velocity of 4.5 cm/s, the relaxation time is 35 s, and the transfer driving force at this time is 2 mg/L, closer to 2.9 mg/L but smaller. Because of the decrease of the oxygen concentration in the gas during the first 50 s (Figure 4a), the mass transfer is lower than that in the ideal case (constant saturation concentration) and the inverse relaxation time τ^{-1} is thus smaller than the mean value of the modeled mass transfer coefficient.

Discussion on Numerical Simulation of Mass Transfer

Now that the model has been validated, numerical results will be used to better understand the mass transfer mechanism in the airlift and the gap between the experimental relaxation time of mass transfer τ^{-1} and the average value of modeled mass transfer coefficient $k_L a_L$.

Liquid-phase perfectly mixed reactor

Indeed, the transport equation of the concentration (Eq. 18) can be reduced to the following equation by surface integration for a steady-state hydrodynamics and a fully developed flow:

$$\frac{\partial\langle\langle\overline{C_L}\rangle\rangle}{\partial t} + \langle\langle\overline{U_Z}\rangle\rangle\frac{\partial\langle\langle\overline{C_L}\rangle\rangle}{\partial Z} = E_{ZL}\frac{\partial^2\langle\langle\overline{C_L}\rangle\rangle}{\partial z^2} + \frac{1}{\langle\alpha_L\rangle}\langle k_L a(C^* - C_L)\rangle \tag{30}$$

The axial dispersion coefficient represents molecular diffusion, turbulent diffusion, and spatial dispersion.[12] The classical equation of the dispersed plug flow model can thus be recognized.

This equation can be nondimensionalized with the following definitions:

$$t^+ = \frac{t}{\tau} \tag{31}$$

where τ is the relaxation time of mass transfer and

$$z^+ = \frac{z}{\langle\langle\overline{U_z}\rangle\rangle t_M} \tag{32}$$

where $\langle\langle\overline{U_Z}\rangle\rangle t_M$ is the length corresponding to the mixing time in the airlift reactor.

Thus, the nondimensional velocity is

$$U^+ = \frac{\langle\langle\overline{U_z}\rangle\rangle\tau}{\langle\langle\overline{U_z}\rangle\rangle t_M} = \frac{\tau}{t_M} \tag{33}$$

The nondimensional concentration is

$$C^+ = \frac{\langle\langle\overline{C_L}\rangle\rangle - C^*}{C^*} \tag{34}$$

assuming C^* constant.

Equation 30 becomes

$$\frac{\partial C^+}{\partial t^+} + \frac{\tau}{t_M}\frac{\partial C^+}{\partial z^+} = \frac{E_{ZL}}{\langle\langle\overline{U_z}\rangle\rangle^2 t_M}\frac{\tau}{t_M}\frac{\partial^2 C^+}{\partial z^{+2}} + \frac{1}{\langle\alpha_L\rangle}\frac{\langle k_L a\rangle}{\tau^{-1}}C^+ \tag{35}$$

The mixing time t_M is equal to several times the circulation time t_C. Let us define

$$t_M = \theta_M t_C \tag{36}$$

and the circulation time is defined by

$$t_C = \frac{2H}{\langle\langle\overline{U_z}\rangle\rangle} \tag{37}$$

The previous equation becomes

$$\frac{\partial C^+}{\partial t^+} + \frac{\tau}{t_M}\frac{\partial C^+}{\partial z^+} = \frac{2}{\theta_M}\frac{\tau}{t_M}\frac{1}{\mathrm{Pe}}\frac{\partial^2 C^+}{\partial z^{+2}} + \frac{1}{\langle\alpha_L\rangle}\frac{\langle k_L a\rangle}{\tau^{-1}}C^+ \tag{38}$$

The first term of the right-hand side clearly vanishes $[(2/\theta_M)(\tau/t_M)(1/\mathrm{Pe}) = 1\%$ for the superficial gas velocity of 1.7 cm/s]. However, the second term of the left-hand side is weighted by the ratio: relaxation time of transfer over macromixing time. For a superficial gas velocity of 1.7 cm/s, this ratio is $60/100 = 0.6$, which is not small compared to unity. For a superficial gas velocity of 4.5 cm/s, this ratio is $35/75 = 0.46$, which is also not small compared to unity. This result can explain the behavior of local oxygen concentration in the liquid vs. time, exhibiting modulation with period equal to the circulation time (Figure 3).

Thus the following transport equation of concentration in the liquid:

$$\frac{\partial\langle\overline{C_L}\rangle}{\partial t} = \frac{1}{\langle\alpha_L\rangle}\langle k_L a\rangle(C^* - \langle\overline{C_L}\rangle) \tag{39}$$

seems oversimplified in the present case of airlift reactor.

Concentration in oxygen in the gas vs. time

Numerical results are given in terms of plots of oxygen concentration in bubble vs. time, at different positions in the airlift and for two superficial gas velocities (Figure 5).

With respect to Figure 5 the curves follow the same trend during the first 10 s. In fact, this behavior is closely related to initial conditions: in the liquid, the initial oxygen concentration is zero everywhere; in the gas, the initial oxygen concentration is fixed at 310 mg/L. Thus, the transfer of oxygen between bubbles and liquid is very important during the first 10 s and, consequently, the concentration of oxygen in the gas decreases rapidly.

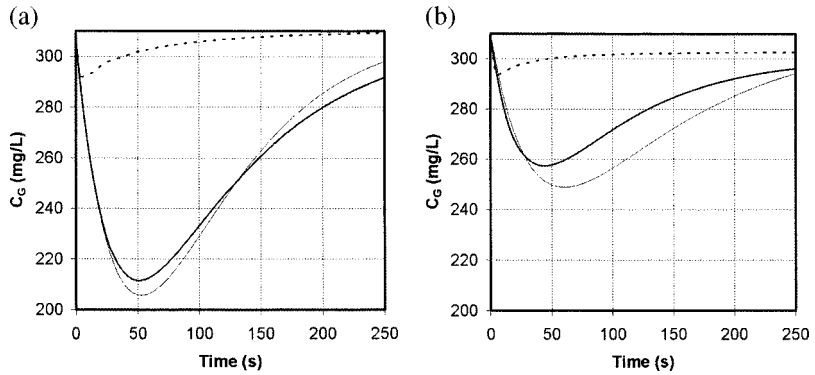

Figure 5. Evolution of computed oxygen concentration in the gas vs. time, in the riser and in the downcomer, for two superficial gas velocities.

—: CFD downcomer, - - -: CFD riser, ⋯⋯: Analytical downcomer.

To confirm this trend, one can solve simplified equations. During the first seconds, neglecting the renewal of gas by the mean flow, Eq. 17 in the gas phase becomes

$$\frac{\partial \alpha_G \overline{C_G}}{\partial t} = -k_L a(m\overline{C_G} - \overline{C_L}) \tag{40}$$

and with reference to Figure 1, the evolution of oxygen concentration in the liquid is $\overline{C_L} = C_L^*[1 - e^{-(k_L a_L)t}]$.

The analytical solution is given by

$$\overline{C_G} = \overline{C_{G0}}\left\{1 + \frac{m\alpha_L}{\alpha_G - m\alpha_L}\left[e^{-(k_L a/\alpha_L)t} - e^{-(mk_L a/\alpha_G)t}\right]\right\} \tag{41}$$

For the superficial velocity of 1.7 cm/s, the analytical solution given by Eq. 41 has been plotted in Figure 5a; agreement with the predicted CFD values is very good, in particular in the downcomer where the bubbles are not renewed. For the superficial velocity of 4.5 cm/s, the analytical solution given by Eq. 41 has been plotted in Figure 5b; the agreement with the predicted CFD values is again very good in the downcomer. Consequently, the behavior predicted in the gas phase in the downcomer is closely related to the fact that the renewal of the bubbles is low.

In the riser, the evolution of oxygen concentration in the gas follows the trend given by Eq. 41 only during the first 10 s. The gas is quickly renewed in the riser. The gas, injected at the bottom of the riser, reaches a height of 2 m after 4 to 5 s. Thus, the decrease of oxygen concentration in the gas in the riser stops after 5 s (Figure 5).

The airlift is well mixed in the liquid phase, and we showed in a previous article[12] that, for a superficial gas velocity of 1.7 cm/s, after four loops, the concentration is uniformly distributed. Thus, after four loops, corresponding to 100 s, the concentration of oxygen in the gas in the riser is almost constant. In the riser, another way to explain this trend is to compare the timescale of renewal of bubbles (about 5 s), which is much smaller than the timescale of mass transfer relaxation (about 60 s at a superficial velocity of 1.7 cm/s and 35 s at a velocity of 4.5 cm/s). In the downcomer, the weak renewal of gas implies that a return to the initial concentration of 310 mg/L will be long, which may be infinitely long in theory if the bubbles are stagnant.

In this part of the experiments, the bubbles transfer the oxygen to the liquid and the oxygen concentration in the bubbles decreases. Then, in the aerated zone of the downcomer, with increasing oxygen concentration in the liquid, the transfer from the liquid to the gas may occur. This will be illustrated by plotting transfer driving force ($C_L^* - C_L$) vs. time.

Mass transfer driving force vs. time

The transfer driving force ($C_L^* - C_L$) is thus tracked to characterize the transfer itself (Figure 6).

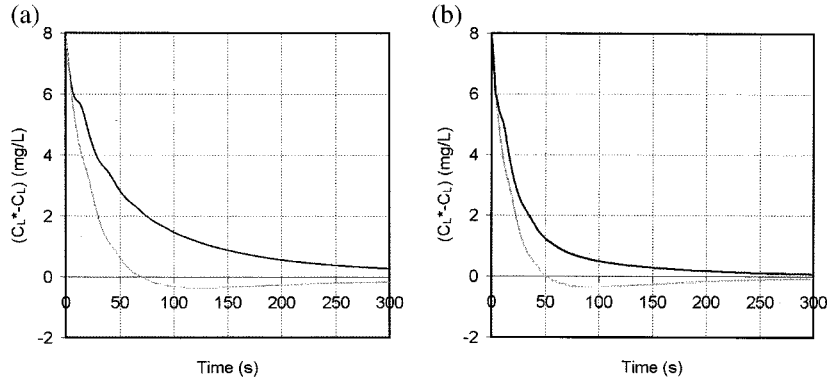

Figure 6. Evolution of computed transfer driving force ($C_L^* - C_L$) vs. time, in the riser and in the downcomer, for two superficial velocities.

—: CFD riser, ⋯⋯: CFD downcomer.

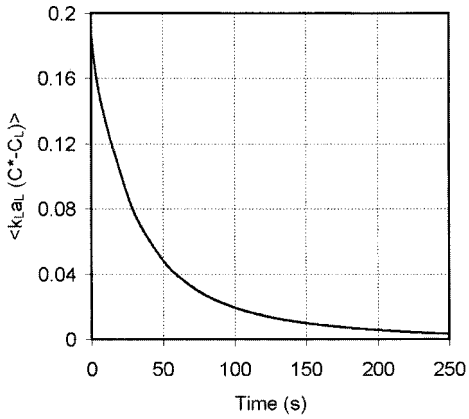

Figure 7. Evolution of $\langle k_L a_L(C^* - C_L)\rangle$.

As mentioned earlier, the behavior predicted in the gas phase in the downcomer is closely related to the fact that the renewal of the bubbles is low. In the first period, the bubbles transfer the oxygen to the liquid and the oxygen concentration in the gas phase decreases. Then, because the concentration of oxygen in the liquid is large, the term $(C_L^* - C_L)$ becomes locally negative (Figure 6) and the concentration of oxygen in the bubbles thus increases by desorption of the liquid. The oxygen concentration in the bubble varies with time, after water deoxygenating. This temporal evolution, which is fast in the riser, makes the transfer driving force $(C_L^* - C_L)$ maximum at initial times and decreases exponentially, with a negative time constant $k_L a_{\text{riser}}^{-1}$. On the contrary, in the aerated zone of the downcomer, the temporal evolution of the oxygen concentration in the gas is strong. The transfer driving force $(C_L^* - C_L)$ of these bubbles is maximum at the beginning, but as the bubble oxygen concentration decreases, this transfer driving force $(C_L^* - C_L)$ decreases as well because C^* decreases and C_L increases. Desorption of the liquid occurs when the transfer driving force $(C_L^* - C_L)$ becomes negative $(C_L^* < C_L)$. This limit time related to bubble desorption can be estimated by equating mC_G to C_L, leading to the relation:

$$t = \frac{\alpha_G \alpha_L}{(k_L a)_{down}(m\alpha_L - \alpha_G)} \ln\left(\frac{m\alpha_L}{\alpha_G}\right) \tag{42}$$

This limit time is of the order of 60 s for the superficial velocity of gas 1.7 cm/s and is 45 s for the superficial velocity of gas 4.5 cm/s, in agreement with Figures 6a and 6b, where CFD predicts, respectively, 72 s (1.7 cm/s) and 50 s (4.5 cm/s).

One can thus assess the quantity of oxygen transferred by the bubbles in the airlift, given that desorption occurs after adsorption, as follows:

$$\int_0^{C^*} dC_L = \int_0^{\infty} k_L a_L (C^* - C_L) dt \tag{43}$$

in the riser and in the downcomer.

The previous integral can also be numerically computed. Figure 7 shows a plot of the time evolution of the spatial average of $k_L a_L(C^* - C_L)$. A numerical integration obviously gives the value of 8 mg/L, which corresponds exactly to C^*.

The bubbles will thus contribute to the transfer efficiency of the airlift, according to their age. This is discussed below.

Bubble age determination

Bubble age ($\overline{T_B}$) or bubble residence time can be determined thanks to the transport equation of a scalar representing residence time of bubble in the airlift loop reactor. At the inlet T_B is 0 s, corresponding to the point where the bubbles are "born" in the reactor. The transport equation of T_B is thus expressed as

$$\frac{\partial \overline{T_B}}{\partial t} + \nabla \cdot \overline{T_B}\,\overline{U_G} = 1 \tag{44}$$

Figure 8a presents the bubble age in the riser for gas superficial velocities of 1.7 and 4.5 cm/s. At the top of the riser, the bubble age is about 5 s. It can also be noticed that bubble age variation is linear with the airlift height, after the establishment zone, which corresponds to about 0.6 m above the injectors. In this zone, recirculation loops occur, causing the bubble to have a slightly higher residence time. The invert of slope is around 0.43 m/s, which is the bubble ascension velocity in the riser, given that the slip velocity is about 0.20 m/s and the liquid velocity is 0.21 m/s. In the downcomer (Figure 8b), bubble residence time is far higher than that in the riser (but not infinite). It also seems that the bubbles near the bubble front are renewed faster (100 s at 1.7 cm/s) than the bubble trapped in the bulk (150 s at 1.7 cm/s). Figure 8b also shows that bubble age is higher for a gas superficial velocity of 4.5 cm/s than of 1.7 cm/s. This can be explained by the fact that the downcomer is more aerated and, because the

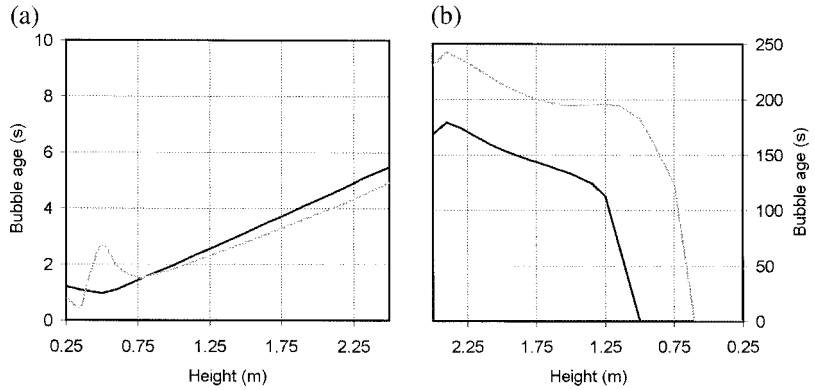

Figure 8. (a) Bubble age in riser; (b) bubble age in downcomer.

— $j_G = 1.7$ cm/s, ⋯ $j_G = 4.5$ cm/s.

liquid and bubble velocity are almost the same as at 1.7 cm/s, then bubbles have a higher residence time.

So, in practice, the bubbles are not stagnant, but have a residence time between the injection and the outlet through the free surface of the airlift. This residence time, very large in the downcomer compared to the 4 or 5 s in the riser, determines the transfer efficiency of the airlift. If this age is one order of magnitude larger than the transfer time, the bubbles are not renewed. These bubbles will weakly contribute to the mass transfer. However, if this age is less than the transfer timescale, the oxygen capacity will be renewed before liquid saturation is reached.

Conclusion on global k_La_L coefficients

From spatial average values of C_L and C_G, a global value of τ^{-1} can also be derived from Eq. 43 using CFD data:

$$\langle C_L \rangle = m\langle C_G \rangle (1 - e^{-t/\tau}) \tag{45}$$

$\tau^{-1}(t)$ can then be expressed by

$$\tau^{-1}(t) = \frac{m\langle C_G(t) \rangle}{\langle C_L(t) \rangle} \int_0^t 1 - \frac{\langle C_L(t) \rangle}{m\langle C_G(t) \rangle} \tag{46}$$

From Eq. 46, the limit value of $\tau^{-1}(t)$ for a gas superficial velocity of 1.7 cm/s is 0.02 s^{-1} and for 4.5 cm/s is 0.04 s^{-1}. These modeled values are in agreement with the experimental value of τ^{-1} calculated in Table 2 (0.017 $\pm$ 0.002 s^{-1} for 1.7 cm/s and 0.035 $\pm$ 0.005 s^{-1} for 4.5 cm/s) and differ from average values of modeled mass transfer coefficient.

Conclusion

The modeling and numerical simulation of mass transfer in an internal airlift loop reactor have been the dual focus of this article. The objective was to validate mass transfer in an internal airlift loop reactor by comparing CFD simulation to experimental results from Couvert[11] by calculating a global mass transfer coefficient (k_La_L). The local bubble interfacial area (a) is sensitive to the bubble shape, in this case ellipsoidal instead of spherical bubble. The eccentricity involves a higher value of a, although the ellipsoidal shape implies that not all the bubble surface is effective for oxygen transfer because of the presence of wake. The local mass transfer coefficient (k_L) can be estimated by the Higbie[13] relation. It is then noticed that inverse global mass transfer relaxation time τ^{-1} is different from the modeled value of k_La_L. Different hypotheses have been disclosed to explain the gap between these two inverse timescales. First, it was demonstrated that oxygen concentration in bubbles (C_G), which is not constant throughout time, thus influences the value of C_L^*, in particular in the downcomer. Second, the fact that the reactor is perfectly mixed is also questioned. Because the characteristic time transfer is of the order of mixing characteristic time involving the equation

$$\frac{dC_L}{dt} = k_La_L(C_L^* - C_L)$$

is oversimplified. This suggests that mass transfer is not uniform in the reactor.

Nevertheless, CFD simulation is able to provide interesting details concerning the bubbles' behavior by calculating their residence time in the reactor, asserting the fact that bubbles are barely renewed in the downcomer part of the reactor, thus decreasing the mass transfer efficiency.

Acknowledgments

The financial support provided by grants from Foundations of Software Engineering and MESR (Ministère de l'Enseignement Supérieur et de la Recherche) is gratefully acknowledged.

Notation

a_p = projected interfacial area, m^2
B_k = gravitational acceleration, m s^{-2}
C_D = drag coefficient
C_k = local statistical averaged concentration in phase k, mg L^{-1}
c_k = local instantaneous concentration in phase k, mg L^{-1}
ck = local instantaneous turbulent component of concentration in phase k, mg L^{-1}
$\langle C_L \rangle$ = cross-section–averaged concentration in phase k, mg L^{-1}
$\tilde{C}_L$ = spatial fluctuation of concentration in phase k, mg L^{-1}
C^* = saturation concentration, mg L^{-1}
$c'u_k$ = turbulent diffusive flux of concentration vector, mg m L^{-1} s^{-1}
D_L = liquid molecular diffusivity, m^2 s
D_{tL} = liquid turbulent diffusivity, m^2 s
D_{dL} = liquid dispersion diffusivity, m^2 s
D_{dL} = liquid numerical diffusivity, m^2 s
E = bubble eccentricity
E_{ZL} = axial dispersion, m s^{-2}
H = height of the internal wall in the airlift reactor, m
j_k = superficial phase velocity, m s^{-1}
k_L = mass transfer velocity, m s^{-1}
k_La = mass transfer coefficient, s^{-1}
L_k = interfacial transfer of concentration between the two phases, mg L^{-1} s^{-1}
m = proportionality coefficient
m_k = local instantaneous interfacial mass transfer, kg m^{-3} s^{-1}
n_{ki} = kth component of the unit vector normal to the interface
Pe = Peclet number (Pe = V_cL/E_{ZL})
R = ideal gas constant, J K^{-1} mol^{-1}
r_b = bubble radius, m
t = time, s
T = temperature, K
t_c = liquid circulation time, s
T_B = bubble residence time, s
U_k = local statistical averaged phase velocity, m s^{-1}
u_k = local instantaneous phase velocity, m s^{-1}
u_k = local instantaneous turbulent component of phase velocity, m s^{-1}
$\langle U_L \rangle$ = cross-sectional averaged phase velocity, m s^{-1}
V_c = liquid circulation velocity, m s^{-1}

Greek letters

α_k = phase retention
δ_i = Dirac function defined at interface locations
ρ_k = phase density, kg m^{-3}
τ_k = viscous stress tensor in phase k, kg m^{-1} s^{-2}

Literature Cited

1. Cockx A, Doquang Z, Liné A, Roustan M. Use of computational fluid dynamics for simulating hydrodynamics and mass transfer in industrial ozonation towers. *Chem Eng Sci*. 1999;54:5085–5090.
2. Cockx A, Doquang Z, Audic J-M, Liné A, Roustan M. Local and global mass transfer coefficients in waste water treatment process by computational fluid dynamics. *J Chem Eng Process*. 2001;40:187–194.

3. Doquang Z, Cockx A, Liné A, Roustan M. Computational fluid dynamics applied to water and waste-water facility modeling. *Environ Eng Policy*. 1999;1–3:137–147.
4. Chisti Y. *Airlift Bioreactors*. New York: Elsevier; 1989.
5. van Benthum WAJ, ven der Lans RGJM, van Loosdrecht MCM, Heijnen JJ. Bubble recirculation regimes in an internal airlift loop reactor. *Chem Eng Sci*. 1999;54:3995–4006.
6. Choi KH, Lee WK. Circulation liquid velocity, gas hold-up and volumetric oxygen transfer coefficient in external-loop airlift reactor. *J Chem Technol Biotechnol*. 1993;56:51–58.
7. Zhang T, Zhao B, Wang J. Mathematical models for macro-scale mass transfer in airlift loop reactor. *Chem Eng J*. 2006;119:19–26.
8. Dhaoudi H, Poncin S, Hornut JM, Wild G, Oinas P, Korpijarvi J. Mass transfer in an external loop airlift reactor: Experiments and modeling. *Chem Eng Sci*. 1997;52:3909–3917.
9. Dhaoudi H, Poncin S, Midoux N, Wild G. Gas–liquid mass transfer in an airlift reactor—analytical solution and experimental confirmation. *Chem Eng Process*. 2001;40:129–133.
10. Choi KH, Chisti Y, Moo-Young M. Comparative evaluation of hydrodynamic and gas–liquid mass transfer characteristics in bubble column and airlift slurry reactors. *Chem Eng J*. 1996;62:223–229.
11. Couvert A. *Etude d'un réacteur airlift rectangulaire à recirculation interne*. PhD Thesis. Toulouse, France: INSA; 2000.
12. Talvy S, Cockx A, Liné A. Modeling hydrodynamics of gas–liquid airlift reactor. *AIChE J*. 2007;53:000–000.
13. Higbie R. The rate of absoprtion of a pure gas into a still liquid during short periods of exposure. *Trans Am Inst Chem Eng*. 1935;35: 365–389.
14. Clift R, Grace JR, Weber ME. *Bubbles, Drops, and Particles*. San Diego, CA: Academic Press; 1978.
15. Lamont JC, Scott DS. An eddy cell model of mass transfer into the surface of a turbulent liquid. *AIChE J*. 1970;16:513–519.
16. Bird RB, Stewart WE, Lightfoot EN. *Transport Phenomena*. New York: John Wiley & Sons; 1960.
17. Darmana D, Deen NG, Kuipers JAM. Detailed modeling of hydrodynamics, mass transfer and chemical reactions in a bubble column using a discrete bubble model. *Chem Eng Sci*. 2005;60:3383–3404.
18. Blanco A, Magnaudet J. The structure of the axisymmetric high Reynolds number flow around and ellipsoidal bubble of fixed shape. *Phys Fluids*. 1995;7:1265–1274.

Manuscript received Jul. 27, 2006, and revision received Nov. 17, 2006.